










Evidence of Fermi surface reconstruction at the metamagnetic transition of the strongly correlated superconductor UTe₂

Q. Niu ¹, G. Knebel ¹, D. Braithwaite ¹, D. Aoki,^{1,2} G. Lapertot,¹ M. Vališka ¹, G. Seyfarth ³, W. Knafo ⁴,
T. Helm ^{5,6}, J.-P. Brison ¹, J. Flouquet,¹ and A. Pourret ^{1,*}

¹Université Grenoble Alpes, CEA, IRIG, PHELIQS, F-38000 Grenoble, France

²Institute for Materials Research, Tohoku University, Oarai, Ibaraki 311-1313, Japan

³Université Grenoble Alpes, EMFL, CNRS, Laboratoire National des Champs Magnétiques Intenses (LNCMI), 38042 Grenoble, France

⁴Laboratoire National des Champs Magnétiques Intenses, UPR 3228, CNRS-UPS-INSA-UGA, 143 Avenue de Rangueil, 31400 Toulouse, France

⁵Max Planck Institute for Chemical Physics of Solids, 01187 Dresden, Germany

⁶Dresden High Magnetic Field Laboratory (HLD-EMFL), Helmholtz-Zentrum Dresden-Rossendorf, 01328 Dresden, Germany



(Received 19 March 2020; accepted 16 June 2020; published 3 August 2020)

Thermoelectric power (S) and Hall effect (R_H) measurements on the paramagnetic superconductor UTe₂ with the magnetic field applied along the hard magnetization b axis are reported. The first-order nature of the metamagnetic transition at $H_m = H_{c2}^b = 35$ T leads to drastic consequences on S and R_H . In contrast to the field dependence of the specific heat in the normal state through H_m , $S(H)$ is not symmetric with respect to H_m . This implies a strong interplay between ferromagnetic fluctuations and a Fermi-surface reconstruction at H_m . R_H is very well described by incoherent skew scattering above the coherence temperature T_m corresponding roughly to the temperature of the maximum in the susceptibility $T_{\chi_{\max}}$ and coherent skew scattering at lower temperatures. The discontinuous field dependence of both $S(H)$ and the ordinary Hall coefficient R_0 , at H_m and at low temperature, provides evidence of a change in the band structure at the Fermi level.

DOI: [10.1103/PhysRevResearch.2.033179](https://doi.org/10.1103/PhysRevResearch.2.033179)

I. INTRODUCTION

The recent discovery of unconventional superconductivity (SC) in the uranium chalcogenide paramagnet UTe₂ with a superconducting transition temperature of $T_{SC} \sim 1.6$ K [1–3] opens new perspectives on superconducting topological properties including emergent Majorana quasiparticles at the verge of magnetic and electronic instability. Transport and thermodynamic measurements demonstrated that correlations play an important role in this system, requiring theoretical treatment beyond the local-density approximation approach [2,4–8]. The closeness of UTe₂ to ferromagnetic quantum criticality [9] induces astonishing superconducting properties. Indeed when the magnetic field is applied along the hard b axis at low temperature, superconductivity survives up to an extremely high field, $H_{c2} = 35$ T, where it is destroyed abruptly by the occurrence of a huge metamagnetic transition at $H_m = H_{c2}$ [3,10]. The unconventional superconducting state in this system, i.e., spin-triplet Cooper pairing, has been identified by a small decrease in the NMR Knight

shift [11] and the large H_{c2} exceeding the Pauli-limiting field [1–3]. Furthermore, reentrant superconductivity arises above H_m when the magnetic field is tilted 30° away from the b axis towards the c axis [10]. The metamagnetic transition occurring at H_m with a jump in the magnetization of $0.6 \mu_B$, when the system enters the polarized paramagnetic state (PPM) [10,12,13], is in agreement with a characteristic energy scale given by the temperature of the maximum in the susceptibility of $T_{\chi_{\max}} \approx 35$ K [14] and the maximum of the Hall effect (R_H) [4]. Furthermore, fluctuations are strongly enhanced through H_m despite the first-order nature of the metamagnetic transition below the critical end point (CEP) at $T_{CEP} \approx 7$ K [12,14].

By some aspects, UTe₂ has properties similar to those found in the unconventional ferromagnetic superconductor URhGe [15]. It shows similar field enhancement of the Sommerfeld coefficient γ (linear T term of the specific heat) associated with reentrant superconductivity when approaching H_m ($H_m = H_r \approx 11.75$ T in URhGe) [16–18]. In URhGe, the metamagnetic transition is connected to a Fermi-surface instability [19,20] which may drive the SC [21,22]. In UTe₂ as well as in URhGe, the metamagnetic transition occurs for the field along the hard magnetization axis. In both systems the metamagnetic transition is strongly connected to the field enhancement of the SC. A major difference is that URhGe is ferromagnetic with a Curie temperature of $T_C = 9.5$ K at $H = 0$ while UTe₂ remains paramagnetic (PM) at least down to 20 mK [23,24].

*alexandre.pourret@cea.fr

Published by the American Physical Society under the terms of the [Creative Commons Attribution 4.0 International license](https://creativecommons.org/licenses/by/4.0/). Further distribution of this work must maintain attribution to the author(s) and the published article's title, journal citation, and DOI.

A key question is the respective roles of ferromagnetic fluctuations and Fermi-surface instabilities at the metamagnetic transition where the SC is abruptly suppressed. Indeed, the large steplike increase of the residual term of the resistivity, ρ_0 , at the metamagnetic transition suggests that, in addition to magnetic fluctuations, a change in the carrier density may occur at the metamagnetic transition for $H \parallel b$ [14]. For this purpose, we investigated the temperature and magnetic field dependencies of the Seebeck coefficient (S) up to 36 T and the Hall resistance (R_H) up to 68 T of UTe_2 for $H \parallel b$. Reentrant superconductivity is observed in both S and R_H close to H_m around 1 K, consistent with resistivity results [3]. The drastic changes in S and in the ordinary Hall effect (R_0) at H_m point to a Fermi-surface reconstruction, contrasting with the rather symmetric behavior of the γ term [12] and of the A coefficient (the T^2 term of the resistivity) through H_m [14].

II. EXPERIMENTAL DETAILS

Single crystals of UTe_2 were grown by chemical vapor transport with iodine as the transport agent. The orientation of the crystals has been verified by Laue diffraction. We performed the S , ρ , and R_H measurements on three samples labeled S1, S2, and S3 with a residual resistivity ratio ($RRR = \frac{\rho(300K)}{\rho(1.5K)}$) of 30, 30, and 22, respectively. The samples were prepared for experiments with heat or electric current along the a axis and the magnetic field along the b axis. S and R_H have been measured on sample S1 using a standard “one heater–two thermometers” setup, and ρ_{xx} and R_H have been measured on samples S2 and S3 with a standard six-point method. The temperature and field dependencies of different transport properties have been measured at the LNCMI Grenoble using a ^3He cryostat up to 36 T and on sample S3 at the LNCMI Toulouse in a pulsed field up to 68 T and temperatures down to 1.5 K.

III. RESULTS AND DISCUSSION

A. Thermoelectric power

Figure 1 shows the magnetic field dependence of S from 0 to 36 T [panel (a)] and from 32 to 36 T [panels (b) and (c)] at various temperatures. At 0.7 K, S is equal to zero up to the first-order transition at $H_m = 34.6$ T, where S shows a clear negative jump followed by a rapid increase in agreement with the collapse of SC above H_m . At the slightly higher temperature 0.86 K, the sample enters the normal state at about 13 T with a negative S , as indicated by the arrows in the inset of Fig. 1(a). A field-induced reentrant superconductivity phase is then observed between 27 and 34.6 T. The first-order character of the transition is also observed in our $S(H)$ measurements with a strong hysteresis (see Fig. 2). Upon warming, the hysteresis closes and the jump vanishes, indicating that the first-order transition terminates at a CEP with $T_{CEP} \approx 7$ K in agreement with previous measurements [12,14]. Below T_{CEP} , there is a slight increase of $|S(H)|$ on approaching H_m , and then $S(H)$ changes abruptly at H_m . Interestingly, the negative jump at H_m disappears at 3.4 K and it becomes positive at higher temperatures, as shown more clearly in Fig. 3(a), where we plot $\Delta S(H_m)/T$ as a function of temperature up to 5 K. The amplitude of the

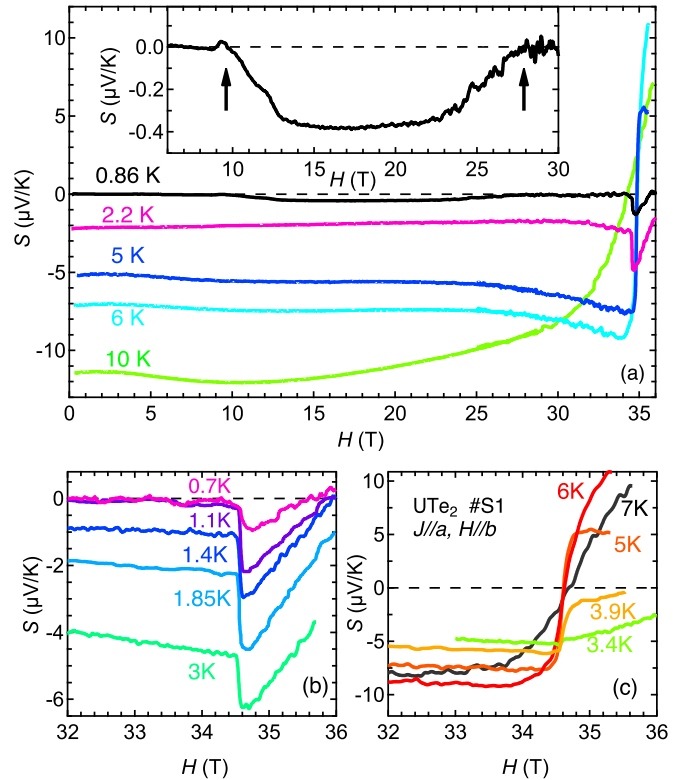


FIG. 1. Field dependence of S in UTe_2 for $H \parallel b$ between 0 and 36 T (a) and between 32 and 36 T (b, c). $S(H)$ shows a clear anomaly at $H_m = 34.6$ T, which broadens with increasing temperature. This anomaly changes from a negative to a positive jump above 3.5 K. The inset in panel (a) shows the reentrant superconductivity in $S(H)$ at 0.86 K in the field range from 6 to 30 T.

transition increases up to $\approx 3 \mu\text{V}/\text{K}^2$ at 5 K. For $T = 10$ K, above T_{CEP} only a large crossover can be detected.

Figure 3(b) shows the temperature dependence of $S(T)/T$ between 0 and 7 K for different magnetic fields. For $H < H_m$ (solid symbols), $S(T)/T \approx 1 \mu\text{V}/\text{K}^2$ is temperature independent in the normal state in this temperature range and for a

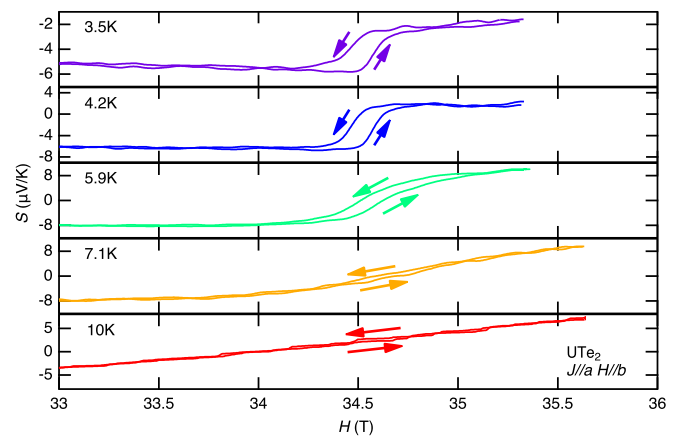


FIG. 2. Temperature evolution of the hysteresis observed in S at H_m . The arrows indicate the direction of the field sweep. The first-order transition ends at the critical end point $T_{CEP} \approx 7$ K.

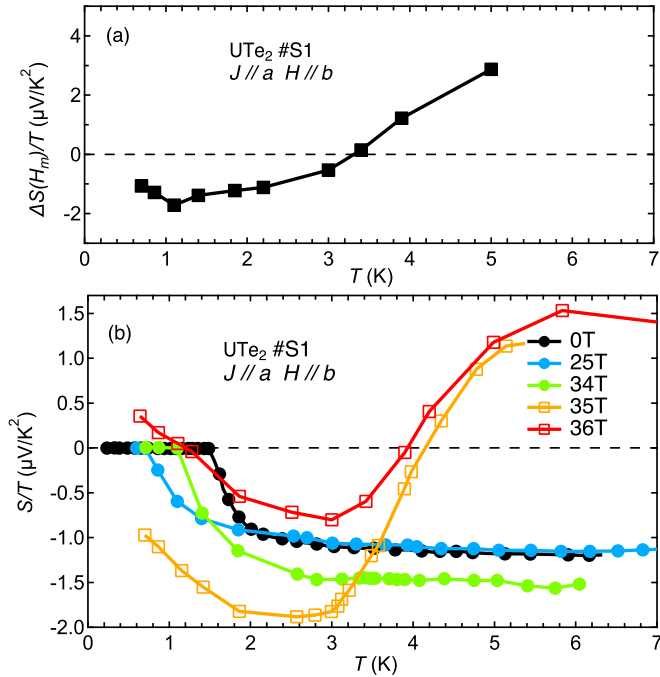


FIG. 3. (a) Magnitude of the jump $\Delta S/T = \frac{S(H_m + \delta H) - S(H_m - \delta H)}{T}$ in S/T at H_m . (b) Temperature dependence of S/T at different magnetic fields (solid symbols, $H < H_m$; open symbols, $H > H_m$). S/T changes drastically with temperature near H_m .

field below 24 T. $|S(T)/T|$ is slightly larger on approaching H_m as shown for 34 T. In contrast, $S(T)/T$ displays a very different temperature dependence above H_m (open symbols). For instance, at 35 T, $S(T)/T < 0$ at low temperature (SC is suppressed) and decreases up to 3 K. Above 3 K, it increases drastically and changes sign at around 4.1 K. Moreover, at 36 T, the interesting feature is that S/T becomes positive at very low temperature below 1.4 K. This shows that at low temperature the sign of the dominant heat carriers changes through H_m from electrons to holes.

B. Hall effect

To extract more information about the field dependence of the carriers across H_m , we measured the Hall effect up to 36 T on sample S2 in the static field and up to 68 T on sample S3 in the pulsed field. Figures 4(a) and 4(b) show the field dependence of the Hall resistivity ρ_{xy} measured on S2 at different temperatures. At 0.45 K, the sample is superconducting up to the metamagnetic transition. Above H_m , ρ_{xy} is positive in the normal state. At 1 K, reentrant superconductivity is detected in ρ_{xy} as indicated by the arrows. However, a negative ρ_{xy} shows up in the normal state below the reentrant superconductivity. As the temperature increases, the transition in ρ_{xy} at H_m becomes huge with a maximum value at 7.5 K near the CEP. At the same time, the initial slope of $\rho_{xy}(H)$ at low field also increases rapidly from negative to positive. The inset of Fig. 4(a) illustrates the temperature dependence of the Hall coefficient $R_H = \rho_{xy}/H$ at different fields. At 9 T, where $\rho_{xy}(H)$ is still linear, $R_H(T)$ changes rapidly from negative

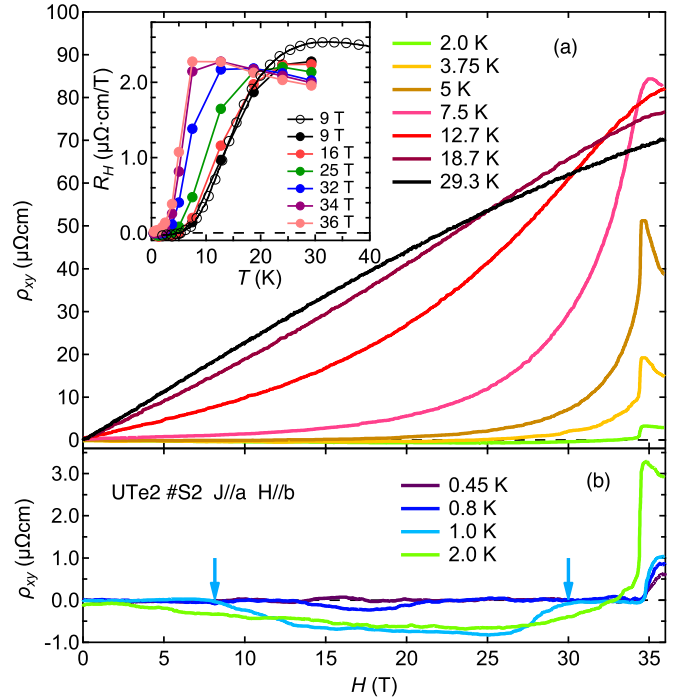


FIG. 4. (a) The Hall resistivity of UTe_2 with $H \parallel b$ up to 36 T at different temperatures. Panel (b) shows a zoom on low temperatures. The arrows indicate the normal state and reentrant superconductivity at 1 K. The inset of panel (a) shows the T dependence of the Hall coefficient at different fields. Previous data are also represented (open circles) [4].

to positive and shows a maximum at $T_m \approx 30$ K close to $T_{\chi_{\max}}$ [4]. This drastic increase of the Hall coefficient at low temperature, which has been observed in many heavy fermion systems, like UPt_3 [25] and UAl_2 [26], is related to the change of the scattering process from incoherent skew scattering at high temperature to a coherent scattering regime at low temperature [27]. As H increases, $R_H(T)$ becomes steeper and T_m shifts to lower temperature until the metamagnetic transition at H_m , where T_m ends at about 7 K close to the CEP (see also Fig. 6). Above H_m , R_H decreases with the field and the temperature where R_H is maximum (labeled T_{cr}) indicates the PM-PPM crossover [19,28]. It shifts to higher temperature when increasing the magnetic field, see also Fig. 9.

In the presence of magnetic fluctuations, R_H can be described by the sum of an ordinary part, R_0 , and an anomalous part, R_S . R_0 is simply related to the density and the mobility of the carriers, while R_S is the result of different scattering processes. In heavy-fermion systems, the incoherent skew scattering of conduction electrons by independent local f moments predominates at high temperature above the coherence temperature [29]. R_S is proportional to the magnetic susceptibility χ and the electrical resistivity ρ_{xx} , i.e., $R_S \propto \rho_{xx}\chi$. This has been verified in many materials in the high-temperature incoherent regime. When the coherence settles in at low temperature, a different scattering mechanism, $R_S \propto \rho_{xx}^2\chi$, has been observed in many uranium heavy-fermion compounds [26], and this is theoretically explained by coherent skew scattering [30].

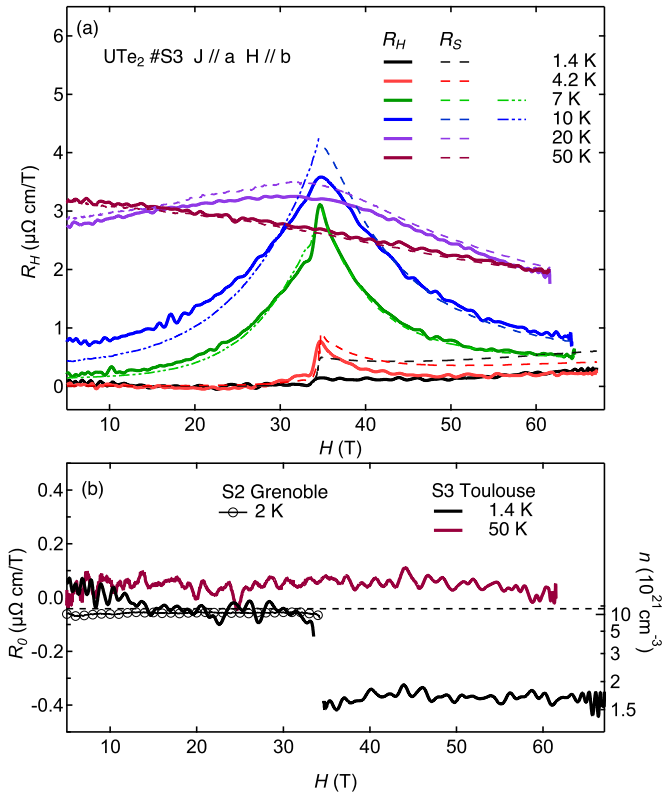


FIG. 5. (a) The Hall coefficient of UTe_2 S3 with $H \parallel b$ up to 68 T (pulsed field). The dashed lines are estimated from the coherent ($T < 20$ K) and incoherent ($T \geq 20$ K) skew scattering at different temperatures. For $T < 20$ K, the long and short dashes correspond to the anomalous Hall signal obtained above and below H_m , respectively. (b) R_0 is obtained after subtracting the anomalous part from the Hall signal (additional temperatures are shown in Fig. 8). The right scale indicates the carrier density and the dashed line represents the value obtained previously [4].

In order to get information on the change of carriers in UTe_2 (for details, see the Appendix), we have used the magnetization data of UTe_2 from Ref. [12] and plotted R_{xy}/H against $R_{xx}M/H$ or R_{xx}^2M/H at different temperatures (see Figs. 11, 12 and 13). R_{xy}/H is linear against R_{xx}^2M/H up to ~ 10 K. However, the curves below and above H_m fall onto two different lines with different slopes and/or intercepts, indicating that both R_0 and R_S have discontinuous changes at H_m . In contrast, at 50 K, which is above T_m , the coherence temperature, R_{xy}/H is on a straight line with $R_{xx}M/H$ in almost the whole field range, consistent with the incoherent skew scattering predictions. The analysis shows that the Hall effect below 10 K is dominated by coherent skew scattering, and the Hall effect above 10 K by incoherent skew scattering. This allows us to estimate the contribution of R_0 to the total Hall effect. The solid lines in Fig. 5(a) show R_{xy}/H , while the dashed lines correspond to the anomalous Hall contribution obtained from the fitting by considering the change of slope of the anomalous Hall effect below (short dash) and above (long dash) H_m . The difference of these two datasets gives an estimation of R_0 as plotted in Fig. 5(b). At 1.4 K, below H_m , R_0 reflects the fact that the anomalous Hall effect vanishes at

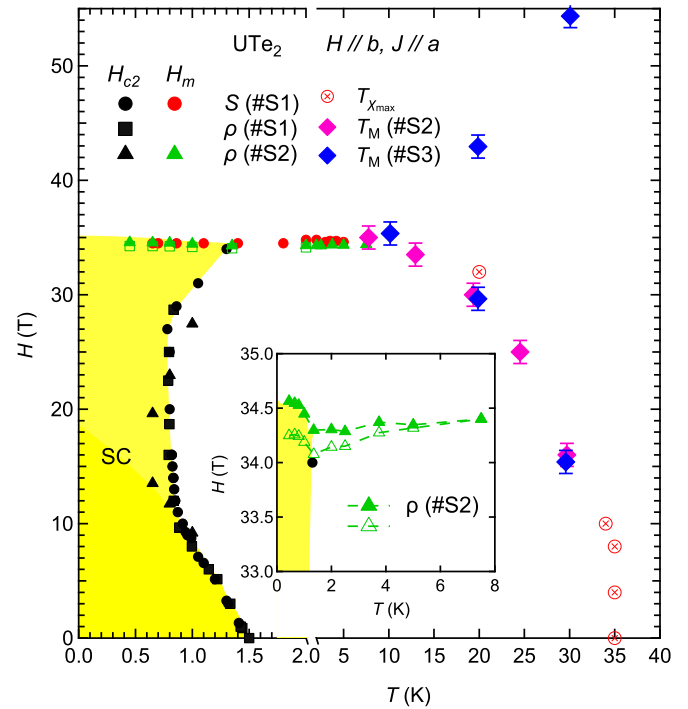


FIG. 6. H - T phase diagram of UTe_2 for $H \parallel b$. H_{c2} from different samples is shown by black symbols, and the metamagnetic field H_m is labeled by red circles (S) and red triangles (ρ). Red crosses, pink diamonds, and blue diamonds indicate $T_{x_{\max}}$, T_m , and T_{cr} , respectively. The inset shows a zoom very close to H_m . Solid symbols are from increasing field sweeps, and open symbols are from downward field sweeps. SC survives slightly above the metamagnetic transition.

low temperature (see also Fig. 10). R_0 is negative, very small, and independent of the magnetic field up to H_m . The value of the extracted carrier density (right scale) is in good agreement with the value obtained previously (dashed line) [4], $n = 1.6 \times 10^{22} \text{ cm}^{-3}$. Above H_m , $|R_0|$ is much larger and still field independent. Most likely, such a behavior is the signature of a change of the carrier density (accompanied or not with a change of the mobility) at the metamagnetic transition. In contrast, at 50 K entering into the incoherent regime, the Hall coefficient can be very well reproduced by anomalous Hall terms.

The upper critical field $H_{c2}(T)$ and H_m detected in S and ρ are summarized in the H - T phase diagram in Fig. 6. $H_{c2}(T)$ is defined by $S = 0$ or $\rho = 0$. Above 10 T, S and ρ show an almost vertical $H_{c2}(T)$ between 10 and 28 T, and H_{c2} is strongly enhanced, reaching 1.4 K at H_m , consistent with previous resistivity experiments [1,3]. The temperatures of the maximum of the Hall effect, T_m (similar to $T_{x_{\max}}$), and T_{cr} are also represented. This is similar to the energy scales observed near the tricritical point in the ferromagnetic superconductor URhGe with the same crossover line separating PM and PPM states [19]. Similar thermoelectric power experiments in the nearly ferromagnetic (FM) case of UCoAl [31] have identified the CEP of the first-order transition at the metamagnetic transition from PM to FM states. This material is an itinerant Ising system, where the metamagnetic transition occurs with H along the Ising axis.

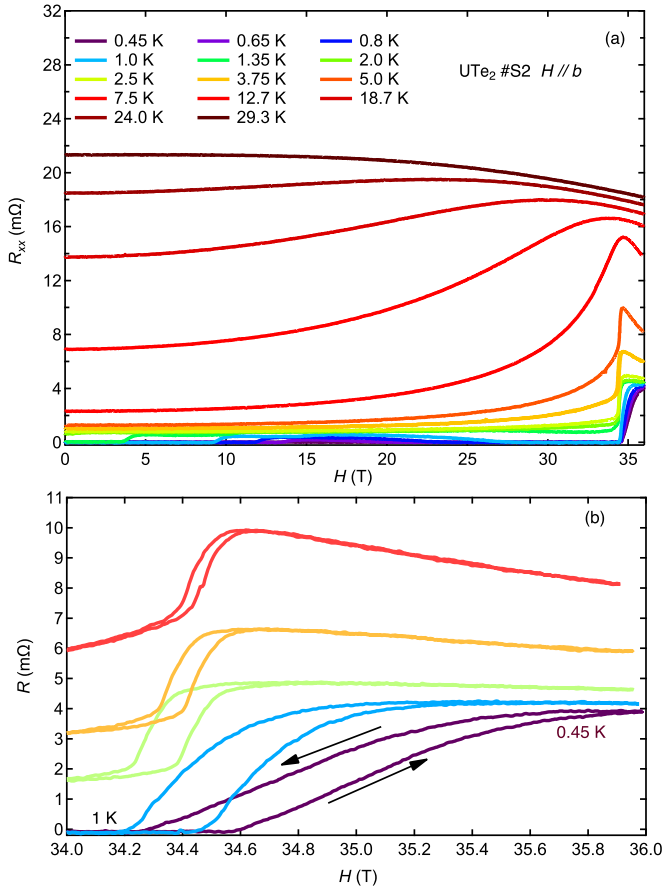


FIG. 7. (a) Field dependence of R_{xx} on sample S2 up to 36 T at different temperatures for $H \parallel b$. (b) Hysteresis loop of R_{xx} at the metamagnetic transition highlighting the first-order character of the transition below $T_{CEP} \approx 7$ K.

In contrast, in UTe_2 as well as in URhGe, the metamagnetic transition occurs for the field along the hard magnetization axis. In both systems the metamagnetic transition is strongly connected to the field enhancement of the SC. The inset magnifies the phase diagram near the metamagnetic transition. We observe that H_m (H_{c2}) has an upturn below 1 K. This feature indicates that SC persists above the extrapolation of H_m to $T = 0$ K, although in a very narrow field range.

IV. CONCLUSION

In conclusion, we have studied the thermoelectric power and the Hall effect of the PM superconductor UTe_2 up to 36 and 68 T, respectively, with the magnetic field along the hard magnetization b axis. Reentrant superconductivity was observed in both S and R_H at low temperature on approaching the metamagnetic transition. R_H is very well described by incoherent skew scattering above the coherence temperature T_M , which corresponds roughly to $T_{\chi_{max}}$, and by coherent skew scattering at lower temperatures. The correspondence of these two energy scales highlights the dual character, localized-itinerant, of the f electrons in uranium compounds. Below this Kondo coherence temperature, density functional theory calculations reveal the emergence of a band structure with a small

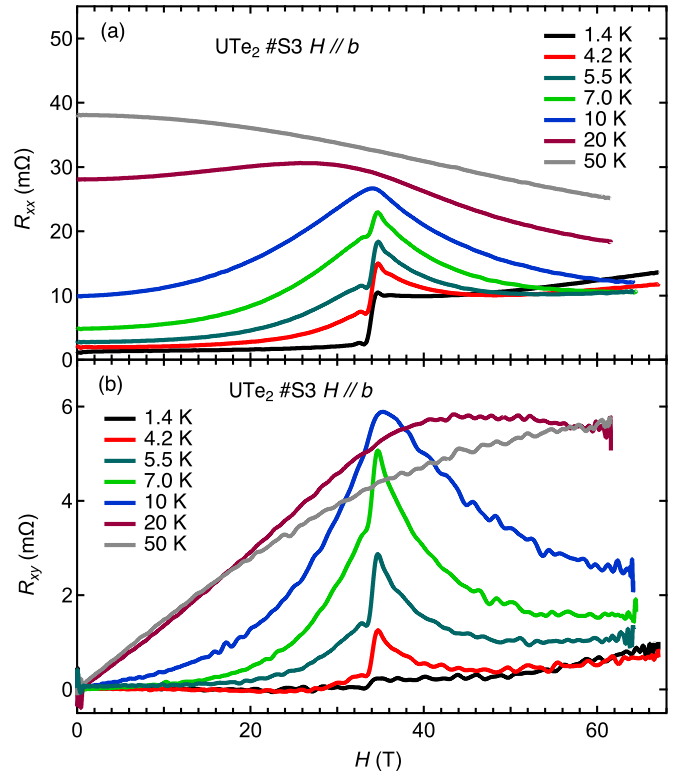


FIG. 8. Field dependence of R_{xx} (a) and R_{xy} (b) on sample S3 up to 68 T at different temperatures.

peak in the density of states at the Fermi level [8]. The field dependence of R_H suggests the suppression of well-defined coherent scattering by strong magnetic fluctuations near the metamagnetic transition. Above T_{SC} , for $H < H_m$, the anomalous part of the Hall signal vanishes, opposite to the case $H > H_m$, where the anomalous part is still present. The strong change of R_0 and S evidences a Fermi-surface reconstruction

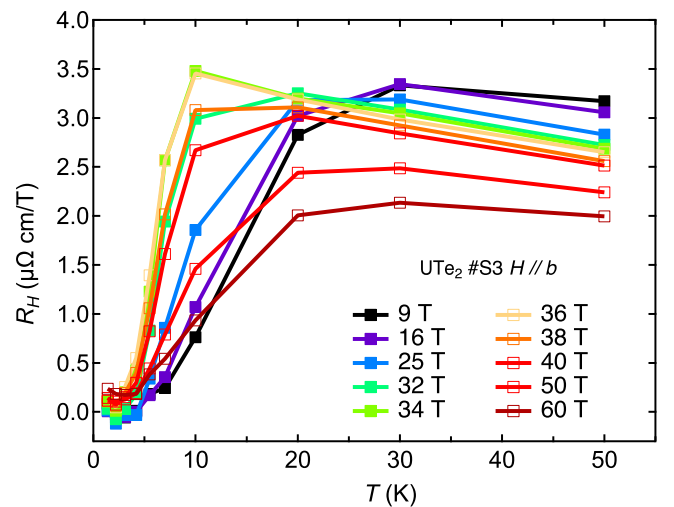


FIG. 9. Temperature dependence of R_H on sample S3 at different magnetic fields for $H < H_m$ (solid symbols) and for $H > H_m$ (open symbols).

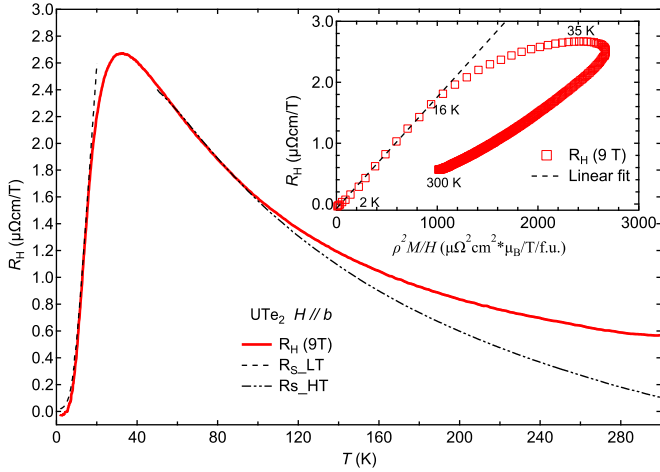


FIG. 10. Temperature dependence of R_H between 1.4 and 300 K. The different fitting curves for the anomalous Hall effect at low temperature ($\propto \rho^2 M/H$) and high temperature ($\propto \rho M/H$) are represented (dashed lines). Inset: R_H as a function of $\rho^2 M/H$. The dashed line represents linear fitting.

at H_m . As this Fermi surface change leads to the vanishing of SC above H_m , a drastic change in the nature of the SC pairing may happen, contrasting with a rather symmetrical variation of $\gamma(H)$ on crossing H_m . A still open question is the anomalous SC phase which persists at 30° from the b axis in the PPM state above H_m . The originality of UTe_2 consists in its proximity to a Kondo-lattice metal-insulator instability which deserves to be studied further under both magnetic field and pressure.

ACKNOWLEDGMENTS

The authors thank K. Izawa, S. Hosoi, H. Harima, J. Ishizuka, and Y. Yanase for stimulating discussions. We acknowledge A. Miyake for high magnetic field magnetization data. This work has been supported by the Université Grenoble Alpes IRS project and KAKENHI (Grants No. JP15H0082, No. JP15H0084, No. JP15K21732, No. JP19H00646, No. JP16H04006, and No. JP15H05745). We acknowledge support of the LNCMI-CNRS, member the European Magnetic Field Laboratory (EMFL).

APPENDIX

1. Resistivity and Hall signal for $H \parallel b$

The resistivity and the Hall effect have been measured on samples S2 and S3, part of the results have been already shown in the main text. Figure 7(a) shows the magnetic field dependence of R_{xx} for different temperatures up to 36 T for sample S2. Below 1.5 K, R_{xx} is zero up to H_m and then shows a steplike anomaly indicating that H_{c2} is equal to H_m

for $H \parallel b$. By increasing temperature, R_{xx} is nonzero below H_m but still shows a steplike anomaly at the metamagnetic transition up to $T_{CEP} \approx 7$ K. Above T_{CEP} , the transition broadens significantly. The first-order character of the transition below T_{CEP} is also confirmed by the observation of a hysteresis loop in the resistivity [see Fig. 7(b)]. Interestingly, as soon as the system becomes superconducting below 1.5 K, the width of the transition broadens and the superconducting transition seems to move to a higher field, conserving a hysteresis loop.

The field dependence of R_{xx} and R_{xy} up to 68 T of sample S3 are represented in Fig. 8. The resistivity data are similar to sample S2. At low temperature, R_{xy} is almost field independent below H_m , shows a small step like anomaly at H_m , and becomes field dependent above H_m . By increasing the temperature, the transition becomes a peak which is very sharp at $T_{CEP} \approx 7$ K and broadens for high temperature. Figure 9 shows the temperature dependence of the Hall coefficient R_H measured on sample S3. Starting from low-magnetic field, the temperature of the maximum in $R_H(T)$, defined as T_m , shifts to low temperature when approaching H_m down to T_{CEP} . Above H_m , the temperature of the maximum T_{cr} , corresponding to the crossover temperature between the PM and PPM state, shifts to higher temperature. The energy scale associated with T_m (similar to $T_{\chi_{max}}$) does not decrease to zero temperature but is limited to T_{CEP} due to the first-order nature of the transition and to the absence of a quantum critical point.

2. Ordinary and anomalous Hall effect

Here we describe the procedure to estimate the ordinary and anomalous contribution to the Hall effect. The first assumption is that the Hall signal is the sum of two terms, $R_H = R_0 + R_S$, where R_0 is the ordinary part associated with the density of carriers and their mobility and R_S is the anomalous part associated with scattering processes on magnetic impurities. The microscopic origin of R_S is quite complex. Three distinct contributions, intrinsic scattering, skew scattering, and side jump scattering have been identified. Each of them has an individual scaling $R_S \propto \rho^\alpha M_z/H$ with respect to the longitudinal resistivity ρ . Here, M_z is the magnetization and H is the magnetic field along the z axis. In ferromagnetic materials, the summation of the three terms yields an empirical formula that explains a large amount of experimental data. However, in heavy fermion materials a satisfactory formula has not been achieved, nevertheless it has been observed that the skew scattering is the dominant scattering process with two different scalings depending on the temperature [27,29]. At high temperature, for $T > T^*$ (coherence temperature), the incoherent skew scattering of conduction electrons by independent f electrons should be considered, and then the relation $R_S = C' \times \rho M/H$ is expected. On the other hand, at low temperature for $T < T_{FL}$ (Fermi liquid temperature) a different scaling is expected, $R_S = C \times \rho^2 M/H$, due to the coherent skew scattering of f electrons once the Fermi

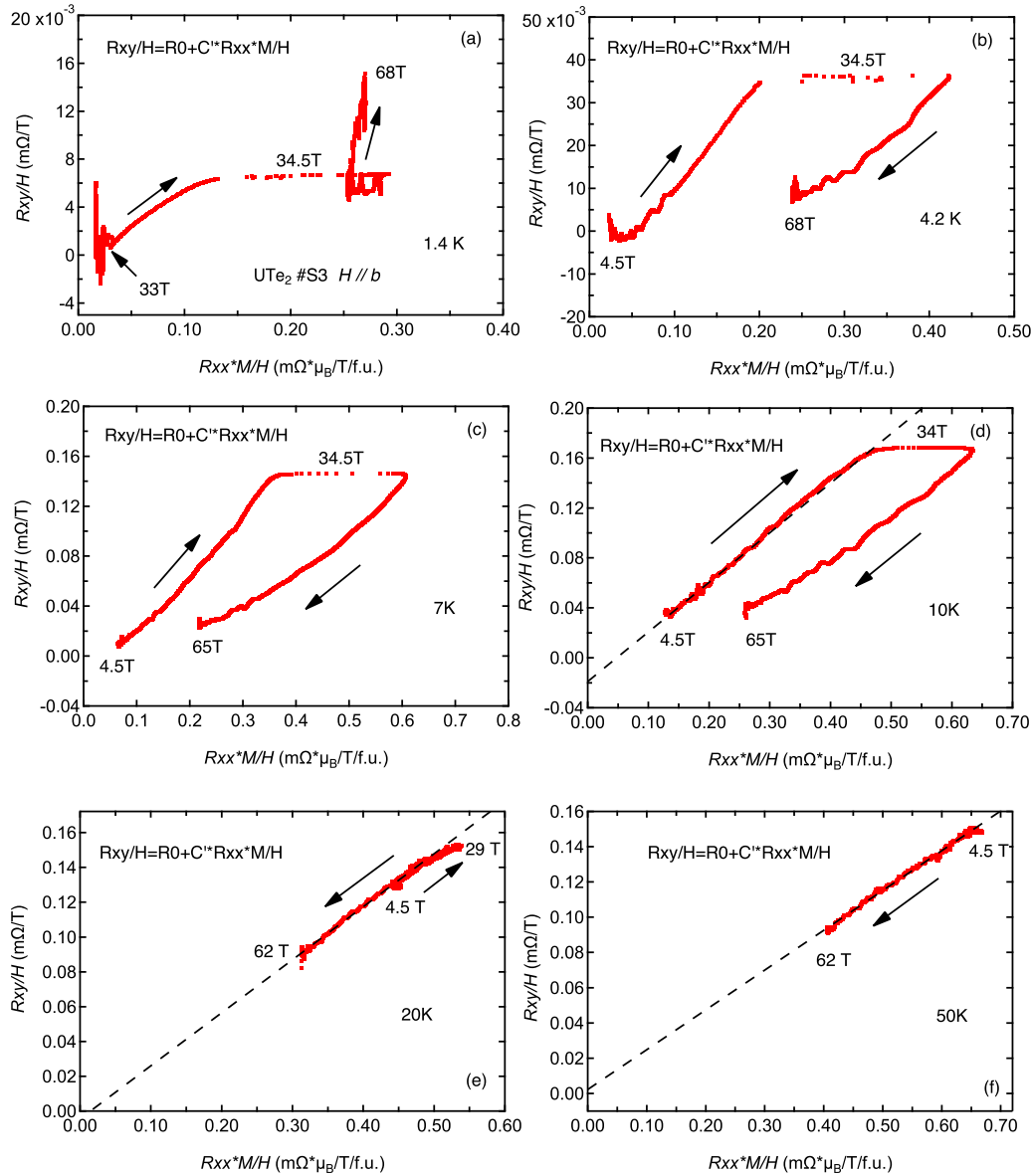


FIG. 11. R_{xy}/H against $R_{xx}M/H$. The dashed lines are linear fits.

surface is well defined. Between T^* and T_{FL} a crossover regime is observed. In Fig. 10, the temperature dependence of R_H is represented. The inset shows that as expected at low temperatures (for $T < 20$ K), the Hall signal is well described by a linear fitting as a function of $\rho^2 M/H$, indicating that below $T_{\chi_{max}}$ a coherent regime appears. The fact that the fit (R_{S_LT}) is smaller than the R_H data at very low temperatures indicates that the anomalous contribution to the Hall signal is negligible at low temperature, and it is justified to extract the number of carriers by using the Hall signal above T_{SC} in this material [4]. The fit using $\rho M/H$ (R_{S_HT}) is not very satisfactory at high temperature. This discrepancy can be explained by the phonon contribution in the resistivity [29].

To extract the coefficients C and C' , we have plotted R_{xy}/H as a function of $R_{xx}M/H$ in Fig. 11 and as a function of $R_{xx}^2 M/H$ in Fig. 12. We observe that for $T < 20$ K, the data are well described by $R_{xx}^2 M/H$, meaning that below T^* (roughly $T_{\chi_{max}}$), the anomalous Hall signal is well described by coherent skew scattering of f electrons. For high temperatures, the anomalous Hall signal is well described by $R_{xx}M/H$ highlighting the predominance of incoherent skew scattering processes above T^* . These observations are summarized in Fig. 13 where R_{xy}/H is plotted either as a function of $R_{xx}M/H$ or as a function of $R_{xx}^2 M/H$ depending on the temperature. It is interesting to notice that for $T > 20$ K, for the whole magnetic field range, the data are well fitted by a unique linear function of $R_{xx}M/H$ passing through the origin, meaning that

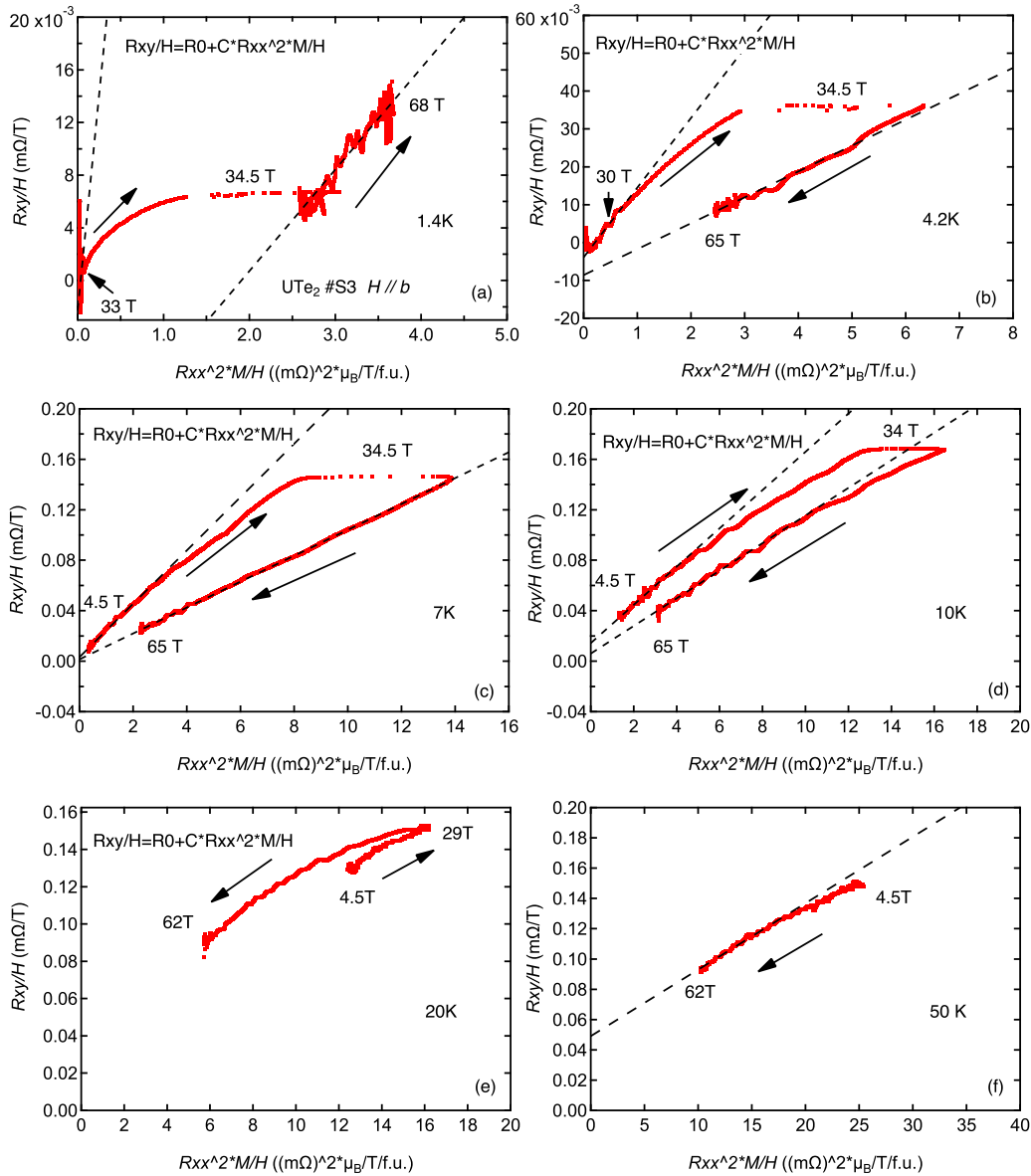


FIG. 12. R_{xy}/H against $R_{xx}^2 M/H$. The dashed lines are linear fits.

the ordinary Hall effect is negligible at high temperatures. At low temperatures, the data are clearly well described by two linear functions of $R_{xx}^2 M/H$ below and above H_m . The value of the coefficients C and C' are summarized in Table I.

The variation of C indicates that the amplitude of the scattering changes through H_m . At 1.4 K, below H_m the data do not show any linear dependence, meaning that the Hall signal is ordinary. On the other hand, above H_m , the data still show linear dependence, meaning that even at very low temperatures, there is still a contribution from the anomalous

Hall effect above the metamagnetic transition just above T_{SC} . After extracting the contribution of the anomalous Hall effect, through the different coefficients C and C' depending on the temperature, we obtained the ordinary contribution by subtracting the anomalous part from the raw data by taking into account the change of the coefficient C through H_m . For all temperatures, the field dependence of the ordinary Hall effect is represented in Fig. 14. A drastic change of the ordinary Hall effect at H_m is extracted from this analysis, indicating a change of the number of carriers associated or not with a change of their mobility.

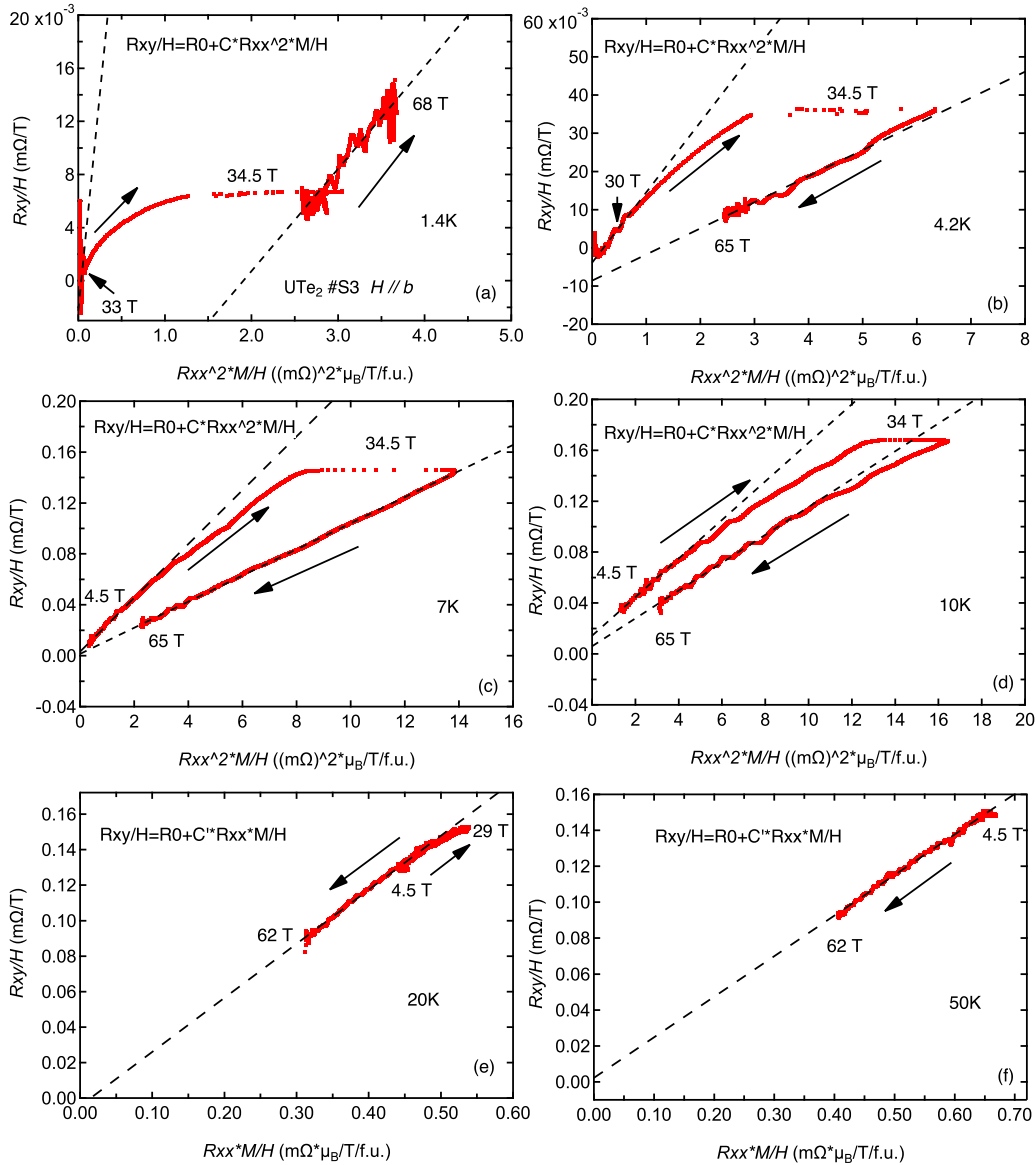


FIG. 13. R_{xy}/H against $R_{xx}^2 M/H$ at 1.4, 4.2, 7, and 10 K. R_{xy}/H against $R_{xx} M/H$ at 20 and 50 K. The dashed lines are linear fits.

TABLE I. List of anomalous Hall effect coefficients C ($R_S = C \times \rho^2 M/H$) for H below and above H_m and C' ($R_S = C' \times \rho M/H$).

T (K)	C (arb. units)		$\frac{C(H > H_m)}{C(H < H_m)}$
	$H < H_m$	$H > H_m$	
1.4	65.3	8.6	0.13
4.2	18.4	7.6	0.41
7	21.1	10.2	0.48
10	13.9	10.5	0.75
	C' (arb. units)		
20	0.30		
50	0.22		

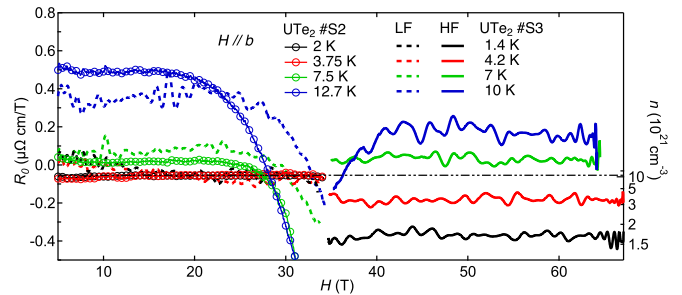


FIG. 14. Complement to Fig. 5(b) of the main text. Ordinary Hall effect as a function of the magnetic field for different temperatures obtained after subtracting the anomalous contribution (taking into account its change of amplitude through H_m). This implies two sets of data for low field (dashed lines, LF) and high field (solid lines, HF) for the sample S3 measured up to 68 T. The right scale indicates the carrier density and the dashed-dotted line represents the value obtained previously [4].

- [1] S. Ran, C. Eckberg, Q.-P. Ding, Y. Furukawa, T. Metz, S. R. Saha, I.-L. Liu, M. Zic, H. Kim, J. Paglione, and N. P. Butch, *Science* **365**, 684 (2019).
- [2] D. Aoki, A. Nakamura, F. Honda, D. Li, Y. Homma, Y. Shimizu, Y. J. Sato, G. Knebel, J.-P. Brison, A. Pourret, D. Braithwaite, G. Lapertot, Q. Niu, M. Vališka, H. Harima, and J. Flouquet, *J. Phys. Soc. Jpn.* **88**, 043702 (2019).
- [3] G. Knebel, W. Knafo, A. Pourret, Q. Niu, M. Vališka, D. Braithwaite, G. Lapertot, M. Nardone, A. Zitouni, S. Mishra, I. Sheikin, G. Seyfarth, J.-P. Brison, D. Aoki, and J. Flouquet, *J. Phys. Soc. Jpn.* **88**, 063707 (2019).
- [4] Q. Niu, G. Knebel, D. Braithwaite, D. Aoki, G. Lapertot, G. Seyfarth, J.-P. Brison, J. Flouquet, and A. Pourret, *Phys. Rev. Lett.* **124**, 086601 (2020).
- [5] J. Ishizuka, S. Sumita, A. Daido, and Y. Yanase, *Phys. Rev. Lett.* **123**, 217001 (2019).
- [6] S.-i. Fujimori, I. Kawasaki, Y. Takeda, H. Yamagami, A. Nakamura, Y. Homma, and D. Aoki, *J. Phys. Soc. Jpn.* **88**, 103701 (2019).
- [7] Y. Xu, Y. Sheng, and Y. F. Yang, *Phys. Rev. Lett.* **123**, 217002 (2019).
- [8] L. Miao, S. Liu, Y. Xu, E. C. Kotta, C.-J. Kang, S. Ran, J. Paglione, G. Kotliar, N. P. Butch, J. D. Denlinger, and L. A. Wray, *Phys. Rev. Lett.* **124**, 076401 (2020).
- [9] Y. Tokunaga, H. Sakai, S. Kambe, T. Hattori, N. Higa, G. Nakamine, S. Kitagawa, K. Ishida, A. Nakamura, Y. Shimizu, Y. Homma, D. Li, F. Honda, and D. Aoki, *J. Phys. Soc. Jpn.* **88**, 073701 (2019).
- [10] S. Ran, I.-L. Liu, Y. S. Eo, D. J. Campbell, P. M. Neves, W. T. Fuhrman, S. R. Saha, C. Eckberg, H. Kim, D. Graf, F. Balakirev, J. Singleton, J. Paglione, and N. P. Butch, *Nat. Phys.* **15**, 1250 (2019).
- [11] G. Nakamine, S. Kitagawa, K. Ishida, Y. Tokunaga, H. Sakai, S. Kambe, A. Nakamura, Y. Shimizu, Y. Homma, D. Li, F. Honda, and D. Aoki, *J. Phys. Soc. Jpn.* **88**, 113703 (2019).
- [12] A. Miyake, Y. Shimizu, Y. J. Sato, D. Li, A. Nakamura, Y. Homma, F. Honda, J. Flouquet, M. Tokunaga, and D. Aoki, *J. Phys. Soc. Jpn.* **88**, 063706 (2019).
- [13] S. Imajo, Y. Kohama, A. Miyake, C. Dong, M. Tokunaga, J. Flouquet, K. Kindo, and D. Aoki, *J. Phys. Soc. Jpn.* **88**, 083705 (2019).
- [14] W. Knafo, M. Vališka, D. Braithwaite, G. Lapertot, G. Knebel, A. Pourret, J.-P. Brison, J. Flouquet, and D. Aoki, *J. Phys. Soc. Jpn.* **88**, 063705 (2019).
- [15] D. Aoki, A. Huxley, E. Ressouche, D. Braithwaite, J. Flouquet, J. P. Brison, E. Lhotel, and C. Paulsen, *Nature (London)* **413**, 613 (2001).
- [16] A. Miyake, D. Aoki, and J. Flouquet, *J. Phys. Soc. Jpn.* **77**, 094709 (2008).
- [17] F. Hardy, D. Aoki, C. Meingast, P. Schweiss, P. Burger, H. v. Löhneysen, and J. Flouquet, *Phys. Rev. B* **83**, 195107 (2011).
- [18] B. Wu, G. Bastien, M. Taupin, C. Paulsen, L. Howald, D. Aoki, and J.-P. Brison, *Nat. Commun.* **8**, 14480 (2017).
- [19] A. Gourgout, A. Pourret, G. Knebel, D. Aoki, G. Seyfarth, and J. Flouquet, *Phys. Rev. Lett.* **117**, 046401 (2016).
- [20] D. Aoki, G. Knebel, and J. Flouquet, *J. Phys. Soc. Jpn.* **83**, 094719 (2014).
- [21] E. A. Yelland, J. M. Barraclough, W. Wang, K. V. Kamenev, and A. D. Huxley, *Nat. Phys.* **7**, 890 (2011).
- [22] Y. Sherkunov, A. V. Chubukov, and J. J. Betouras, *Phys. Rev. Lett.* **121**, 097001 (2018).
- [23] S. Sundar, S. Gheidi, K. Akintola, A. M. Côté, S. R. Dunsiger, S. Ran, N. P. Butch, S. R. Saha, J. Paglione, and J. E. Sonier, *Phys. Rev. B* **100**, 140502(R) (2019).
- [24] C. Paulsen, G. Knebel, G. Lapertot, D. Braithwaite, A. Pourret, D. Aoki, F. Hardy, J. Flouquet, and J. P. Brison, *arXiv:2002.12724*.
- [25] J. Schoenes and J. J. M. Franse, *Phys. Rev. B* **33**, 5138 (1986).
- [26] M. Hadžić-Leroux, A. Hamzić, A. Fert, P. Haen, F. Lapierre, and O. Laborde, *Europhys. Lett.* **1**, 579 (1986).
- [27] Y.-F. Yang, *Phys. Rev. B* **87**, 045102 (2013).
- [28] A. Palacio Morales, A. Pourret, G. Seyfarth, M.-T. Suzuki, D. Braithwaite, G. Knebel, D. Aoki, and J. Flouquet, *Phys. Rev. B* **91**, 245129 (2015).
- [29] A. Fert and P. M. Levy, *Phys. Rev. B* **36**, 1907 (1987).
- [30] K. Yamada, K. Ani, H. Kohno, and S. Inagaki, *Prog. Theor. Phys.* **89**, 1155 (1993).
- [31] A. Palacio-Morales, A. Pourret, G. Knebel, T. Combier, D. Aoki, H. Harima, and J. Flouquet, *Phys. Rev. Lett.* **110**, 116404 (2013).